Supporting Information

Crystal Chemistry and Phonon Heat Capacity in Quaternary Honeycomb Delafossites: $Cu[Li_{1/3}Sn_{2/3}]O_2$ and $Cu[Na_{1/3}Sn_{2/3}]O_2$

Mykola Abramchuk,[†] Oleg I. Lebedev,[‡] Olle Hellman,[¶,†] Faranak Bahrami,[†] Natalia E. Mordvinova,[‡] Jason W. Krizan,[†] Kenneth R. Metz,[§] David Broido,[†] and Fazel Tafti[*,†]

†*Department of Physics, Boston College, Chestnut Hill, MA 02467, USA*

‡*Laboratorie CRISMAT, ENSICAEN-CNRS UMR6508, 14050 Caen, France*

¶*Division of Engineering and Applied Science, California Institute of Technology, Pasadena, CA 91125, USA*

§*Department of Chemistry, Boston College, Chestnut Hill, MA 02467, USA*

E-mail: fazel.tafti@bc.edu

Phone: (617) 552-2127

Controlling the stacking disorder in Na_2SnO_3

Figure S1 shows the stepwise synthesis of Na_2SnO_3 (or equivalently $Na[Na_{1/3}Sn_{2/3}]O_2$). The first solid state reaction at 800 °C ends with a large amount of stacking disorder which appears in the X-ray pattern as an asymmetric broadening of the honeycomb peaks in the region between 18 and 26 degrees. This is improved by annealing the material in 50 °C steps from 800 °C to 1000 °C. At each step, 5% Na_2CO_3 is added to compensate for the volatility of sodium. For the exchange reaction, we used samples with moderate levels of stacking fault (900 °C in Figure S1).

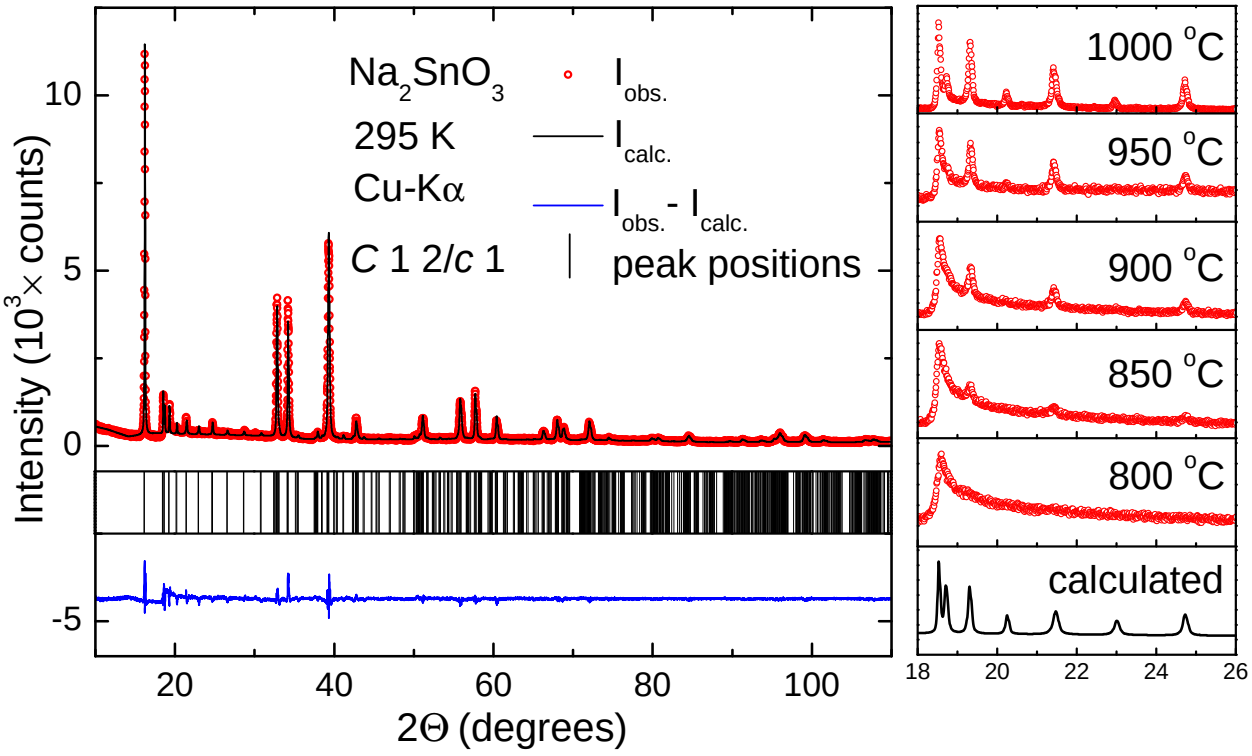

Figure S1: The left panel shows PXRD pattern from a Na_2SnO_3 sample synthesized at 1000 °C. The pattern is refined in the $C2/c$ space group with honeycomb ordering. The honeycomb ordering appears as a series of satellite peaks in the region between 18 and 26 degrees. The right panel shows an asymmetric broadening of the honeycomb peaks in this region. From bottom to top, we plot the calculated pattern of the honeycomb ordering peaks, the broadening of these peaks due to stacking disorder in a sample synthesized at 800 °C, and the subsequent improvement of the stacking order by successive annealing the sample in 50 °C steps until 1000 °C.

Thermal analysis (DSC)

Figure S2(a) shows the differential scanning calorimetry (DSC) analysis on $Cu[Li_{1/3}Sn_{2/3}]O_2$ and $Cu[Na_{1/3}Sn_{2/3}]O_2$. Both compounds start to decompose at approximately 400 °C according to:

$$4Cu[Li_{1/3}Sn_{2/3}]O_2 \rightarrow Li[Li_{1/3}Sn_{2/3}]O_2 + 2Cu_2O + 2SnO_2 \quad (1)$$

$$4Cu[Na_{1/3}Sn_{2/3}]O_2 \rightarrow Na[Na_{1/3}Sn_{2/3}]O_2 + 2Cu_2O + 2SnO_2 \quad (2)$$

The low decomposition threshold is characteristic of metastable phases such as the quaternary delafossites studied here. Therefore, it is necessary to synthesize them under mild conditions (380–400 °C and 24 h).

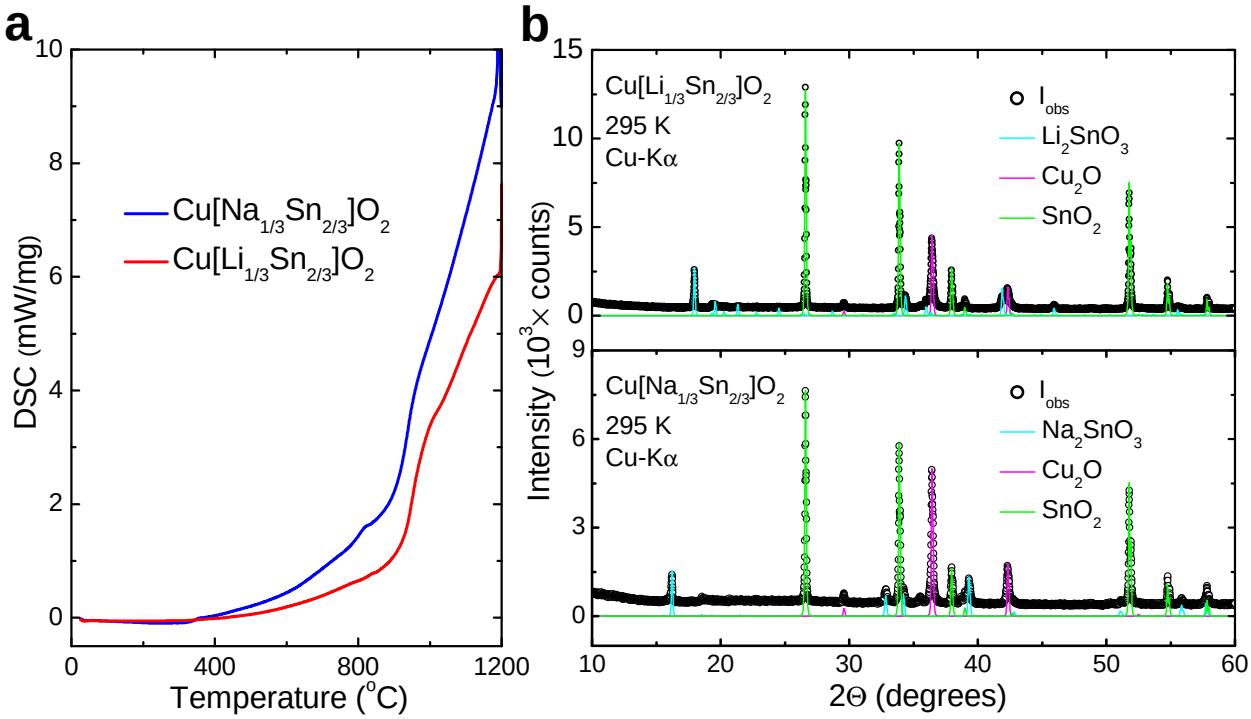

Figure S2: (a) DSC analysis in $Cu[Li_{1/3}Sn_{2/3}]O_2$ (red) and $Cu[Na_{1/3}Sn_{2/3}]O_2$ (blue) under argon atmosphere. Decomposition starts at about 400 °C. (b) Room temperature PXRD patterns after the DSC experiment. Both metastable phases decompose to their thermodynamically stable parent compounds plus tin(IV) and copper(I) oxides.

Effect of the ionic size on the exchange reaction

In the main text, we mentioned that according to size considerations, CuCl (CuI) is the preferred reagent to exchange Li_2SnO_3 (Na_2SnO_3) because Cl^- is a smaller anion compared to I^- and Li^+ is a smaller cation compared to Na^+. This is confirmed in Figure S3 that shows the failure of the following hypothetical reactions:

$$Li[Li_{1/3}Sn_{2/3}]O_2 + CuI \rightarrow Cu[Li_{1/3}Sn_{2/3}]O_2 + LiI \quad (3)$$

$$Na[Na_{1/3}Sn_{2/3}]O_2 + CuCl \rightarrow Cu[Na_{1/3}Sn_{2/3}]O_2 + NaCl \quad (4)$$

The first reaction simply does not proceed (Figure S3a), and the second reaction results in a decomposition of the reagents (Figure S3b). Both reactions were performed under mild conditions (400 °C and 24 h).

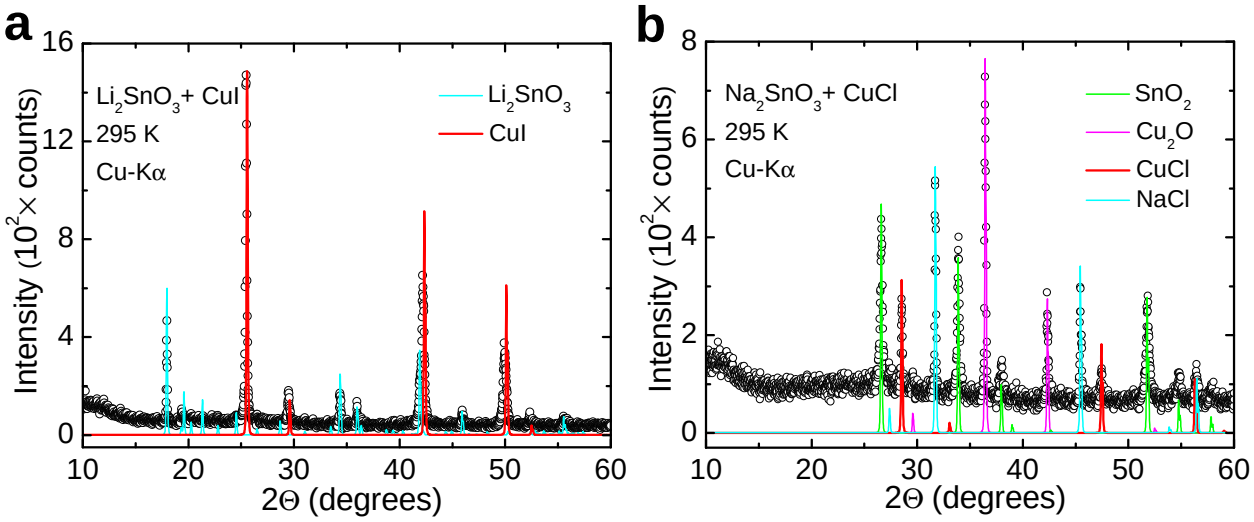

Figure S3: (a) Equation 3 does not proceed. (b) Equation 4 results in a decomposition of the starting reagents instead of producing quaternary delafossites.

Energy dispersive X-ray spectroscopy (EDX)

Figures S4a and S4b show SEM-EDX results from both $Cu[Li_{1/3}Sn_{2/3}]O_2$ and $Cu[Na_{1/3}Sn_{2/3}]O_2$ samples confirming the ratio Cu/Sn = 3/2. Figure S4c shows crystallites from a pressed pow-

der specimen of $Cu[Li_{1/3}Sn_{2/3}]O_2$ under $\times 3000$ magnification. It is not possible to perform a quantitative EDX analysis on lithium due to its small atomic number ($Z = 3$). However, sodium can be detected with a high-resolution detector. Figure S4d shows the EDX analysis on a $Cu[Na_{1/3}Sn_{2/3}]O_2$ sample with a more sensitive EDAX detector where the sodium peak is resolved.

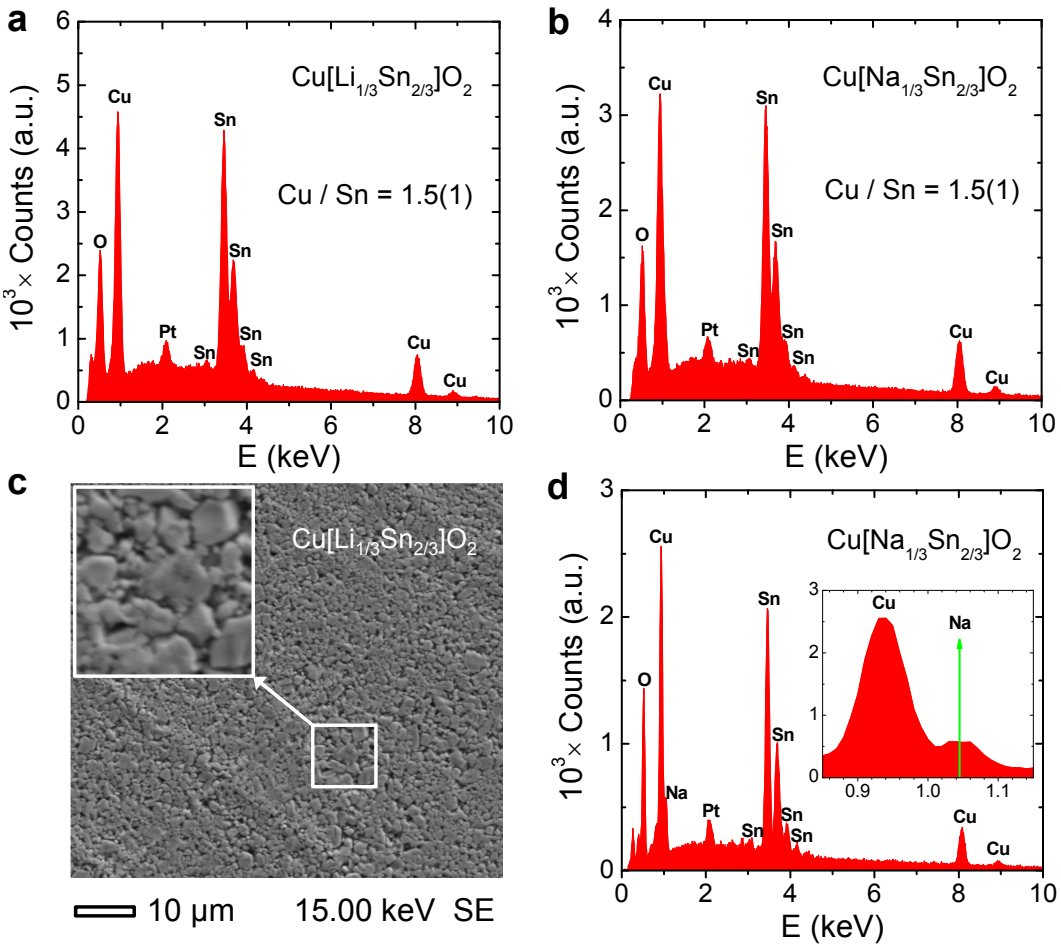

Figure S4: (a) EDX spectrum from a pressed powder specimen of $Cu[Li_{1/3}Sn_{2/3}]O_2$. (b) EDX spectrum from a pressed powder specimen of $Cu[Na_{1/3}Sn_{2/3}]O_2$. (c) SEM image of micron-size crystallites of $Cu[Li_{1/3}Sn_{2/3}]O_2$. (d) EDX spectrum from a pressed powder specimen of $Cu[Na_{1/3}Sn_{2/3}]O_2$ with a higher resolution EDAX detector revealing the sodium peak.

Figure S5 shows elemental maps obtained from crystallites of both $Cu[Li_{1/3}Sn_{2/3}]O_2$ (top panels) and $Cu[Na_{1/3}Sn_{2/3}]O_2$ (bottom panels) using a TEM-EDX technique. Uniform distributions of Cu, Sn, and O are confirmed. The alkali distribution is not presented because Li is invisible to EDX detectors.

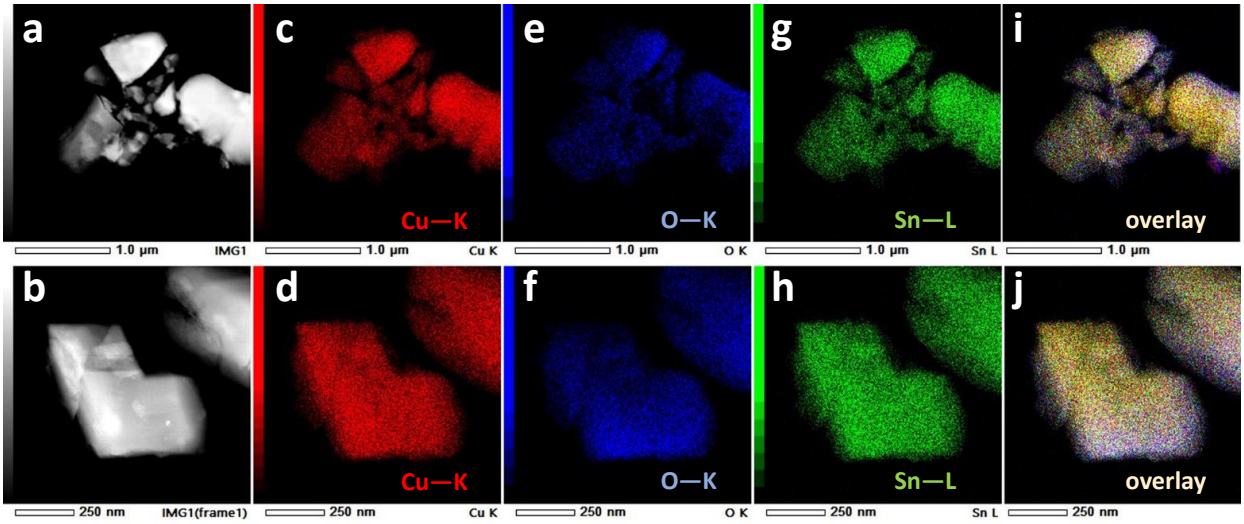

Figure S5: (a,b) Image of the $Cu[Li_{1/3}Sn_{2/3}]O_2$ (top) and $Cu[Na_{1/3}Sn_{2/3}]O_2$ (bottom) crystallites used for the elemental mapping. (c,d) A uniform distribution of copper is confirmed in both materials using TEM-EDX. (e,f) A uniform distribution of oxygen is confirmed in both materials. (g,h) A uniform distribution of tin is confirmed in both materials. (i,j) An overlay of the distribution of Cu, O, and Sn is presented.

Inductively coupled plasma optical emission spectroscopy (ICP-OES)

Figures S6(a–c) show linear regressions on nine standards used to determine the stoichiometry of Cu, Li, and Sn in $Cu[Li_{1/3}Sn_{2/3}]O_2$. A similar analysis is performed on $Cu[Na_{1/3}Sn_{2/3}]O_2$ as shown in Figures S6(d–f).

Rietveld refinement in $C2/m$ space group

In the main text, we presented refinements of both title compounds in the space group $C2/c$. In Figure S7, we present refinements of both systems in a closely related space group $C2/m$. Honeycomb delafossites are commonly refined in either space groups $C2/c$ and $C2/m$ which are difficult to distinguish without having single crystal data. The advantage of $C2/m$ is that it offers a simpler model with a smaller unit cell which make calculations easier. Table S1 shows that the quality of refinements in $C2/m$ (SG 12) are comparable to the goodness of fits in $C2/c$ (SG 15). The inset of Figure S7(a) visualizes the single layer unit cell in space group $C2/m$ that is simpler than the double layer unit cell in space group $C2/c$. It is tempting

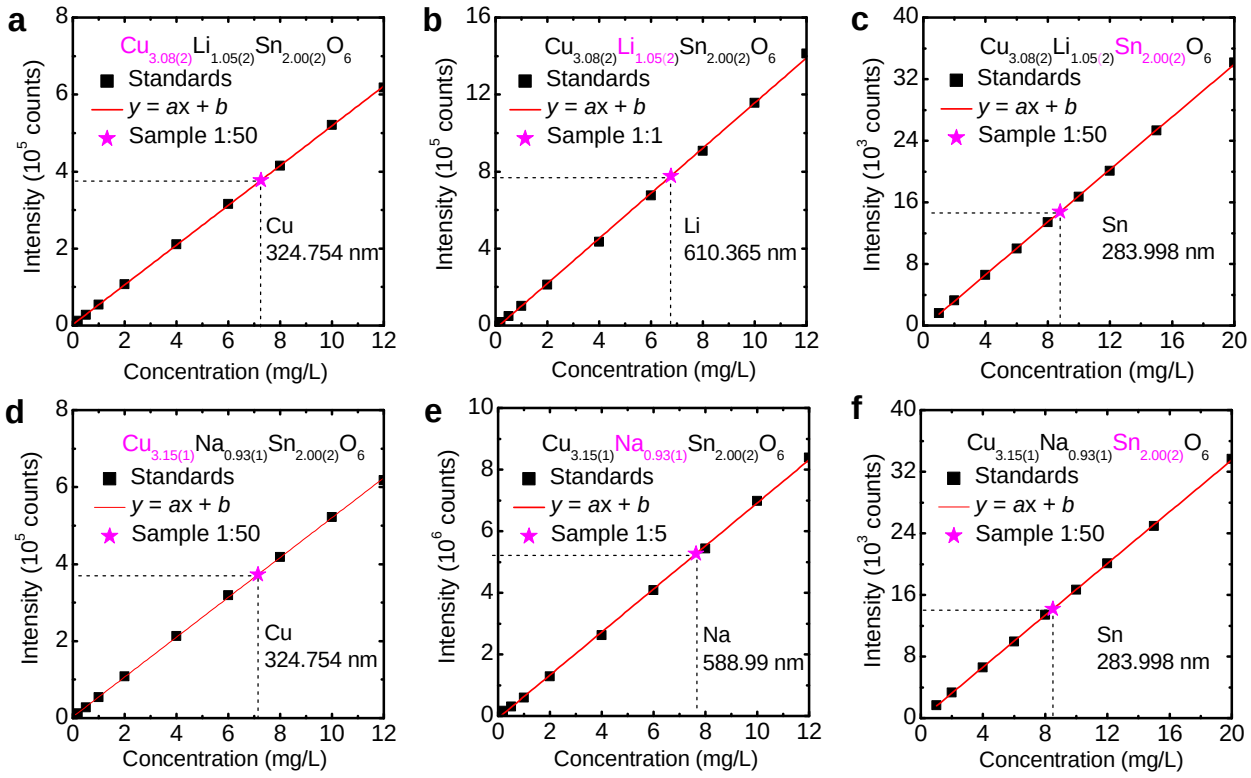

Figure S6: (a) Spectroscopic data points were collected from nine standards. The magenta star is the data point from the sample and the dashed lines show the concentration (mg/L) and the intensity of the emission line from the sample. The emission line at 324.754 nm was used to determine the copper content in the sample. The experimental uncertainty in the reported value comes from a linear direct calibration plot. A similar analysis was performed to determine the lithium (b) and tin (c) content in $Cu[Li_{1/3}Sn_{2/3}]O_2$. Similarly, ICP-OES was used to determine the copper (d), sodium (e), and tin (f) contents in $Cu[Na_{1/3}Sn_{2/3}]O_2$.

to accept the $C2/m$ refinement based on the simplicity of this model; however, the inset of Figure S7(b) shows that the honeycomb ordering in this space group is incomplete and disagrees with our TEM images of the lattice. Therefore, the $C2/m$ model yields a simple but incomplete description of the structure and the correct space group is $C2/c$. Furthermore, we experienced difficulty in converging the refinement in the $C2/m$ space group and could not refine all parameters simultaneously which is a typical sign of an unstable refinement.

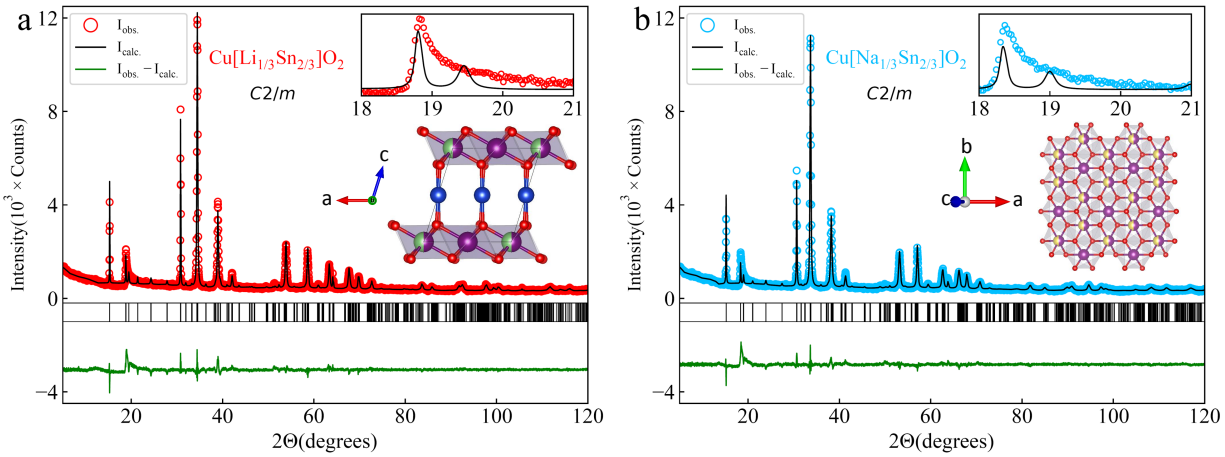

Figure S7: (a) Rietveld refinement of $Cu[Li_{1/3}Sn_{2/3}]O_2$ in the space group $C2/m$. The inset gives a view of the unit cell down the b–axis. Table S2 summarizes atomic positions and occupancies. (b) Rietveld refinement of $Cu[Na_{1/3}Sn_{2/3}]O_2$ in the space group $C2/m$. The inset gives a view of the unit cell down the c–axis revealing a wrong honeycomb pattern.

Residual linear term in heat capacity

As explained in the main text, we were particulalry interested in non-magnetic insulators without any contributions from conduction electrons or magnons to the heat capacity. This is emphasized in Figure S8 which is a plot C/T as a function of T^2 (and T) in both title compounds and shows the absence of a residual linear term that could originate from either conduction electrons or magnons.

Table S1: Unit cell dimensions and refinement parameters from a fit to $C2/m$ space group.

Material	$Cu[Li_{1/3}Sn_{2/3}]O_2$	$Cu[Na_{1/3}Sn_{2/3}]O_2$
Mass (gr/mol)	176.99	182.34
Space group	$C12/m1$	$C12/m1$
a (Å)	5.4590(0)	5.5926(1)
b (Å)	9.4316(1)	9.6719(2)
c (Å)	6.0786(1)	6.1170(1)
β (°)	107.321(2)	107.514(3)
V (Å^3)	298.788	315.539
Z	6	6
D (gr/cm^3)	5.907	5.761
T (K)	295	295
R_{Bragg}	13.7	12.0
R_{f}	9.54	8.89
R_{exp}	4.17	4.16
R_{p}	6.35	5.70
R_{wp}	9.30	8.54
χ^2	4.98	4.22

Table S2: Wyckoff sites, atomic coordinates, and site occupancies from a refinement in the $C2/m$ space group. Note there are no Li/Na atoms in site $2b$. When we try to refine by adding alkali atoms to this site, we get an occupancy less than 0.05 which is practicaly zero.

		$Cu[Li_{1/3}Sn_{2/3}]O_2$			$Cu[Na_{1/3}Sn_{2/3}]O_2$			
Atom	site	x	y	z	x	y	z	occupancy
Cu1	$2c$	0	0	1/2	0	0	1/2	1.000
Cu2	$4h$	0	0.340	1/2	0	0.340	1/2	1.000
Sn1	$4g$	0	0.1601(5)	0	0	0.1591(4)	0	0.500
Li,Na	$4g$	0	0.1601(5)	0	0	0.1591(4)	0	0.500
Sn2	$2b$	0	1/2	0	0	1/2	0	1.000
O1	$8j$	0.881	0.343	0.172	0.881	0.343	0.172	1.000
O2	$4i$	0.916	0	0.183	0.916	0	0.183	1.000

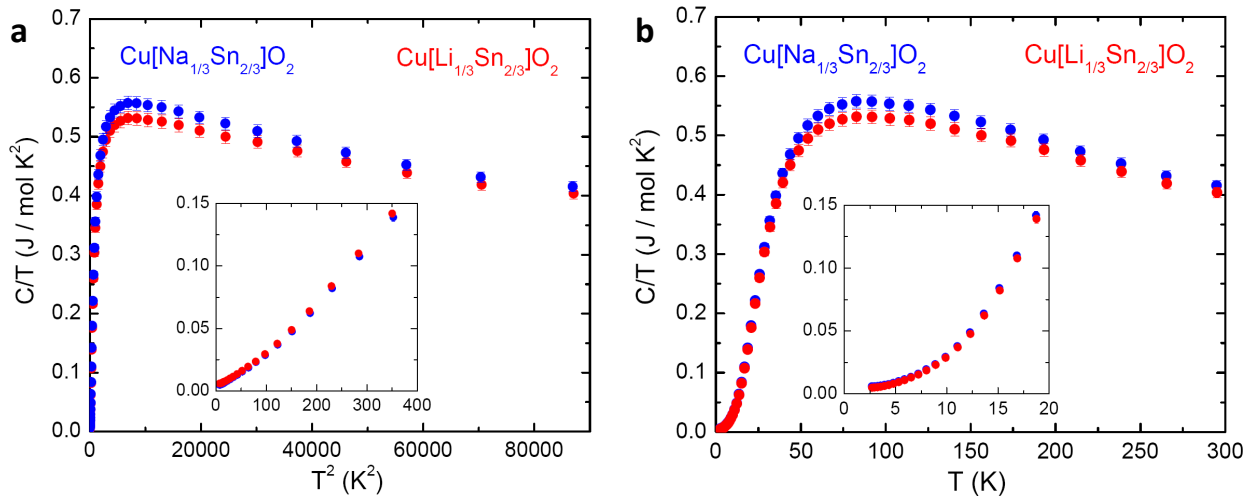

Figure S8: (a) C/T plotted as a function of T^2 to show the absence of a residual linear term in the heat capacity of $Cu[Na_{1/3}Sn_{2/3}]O_2$ and $Cu[Li_{1/3}Sn_{2/3}]O_2$. (b) C/T plotted as a function of T to make the low temperature data more visible.

Phonon dispersions

Figure S9 shows phonon dispersions plots for $Na[Na_{1/3}Sn_{2/3}]O_2$, $Cu[Na_{1/3}Sn_{2/3}]O_2$, $Li[Li_{1/3}Sn_{2/3}]O_2$, and $Cu[Li_{1/3}Sn_{2/3}]O_2$. Density of states is calculated by adding the number of allowed states (according to dispersion curves) at each frequency. Notice that the acoustic branches of the copper-exchanged systems are less dispersive due to the heavier mass of copper compared to the alkali.

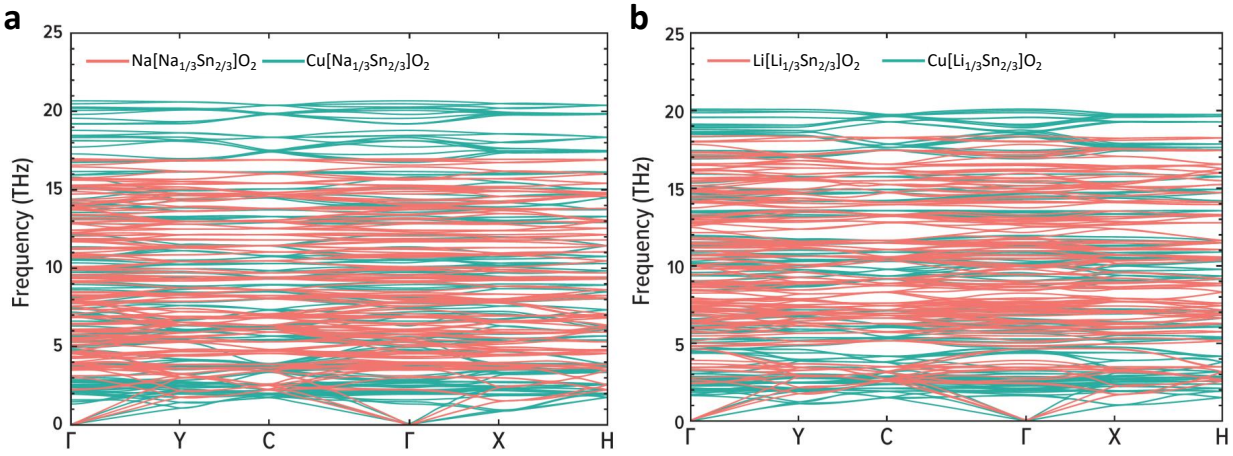

Figure S9: (a) Phonon dispersions for $Na[Na_{1/3}Sn_{2/3}]O_2$ and $Cu[Na_{1/3}Sn_{2/3}]O_2$. (b) Phonon dispersions for $Li[Li_{1/3}Sn_{2/3}]O_2$ and $Cu[Li_{1/3}Sn_{2/3}]O_2$.